



Compact TE-pass polarizer based on silicon-on-insulator platform with bimetallic rhodium–silver grating

Ola Youssef M. Hiza¹ · B. M. Younis^{2,3} · Nihal F. F. Areed^{1,2} ·
Mohamed Farhat O. Hameed^{2,4,5} · S. S. A. Obayya^{1,2}

Received: 29 December 2022 / Accepted: 2 March 2023 / Published online: 8 April 2023
© The Author(s) 2023

Abstract

An ultra-compact hybrid plasmonic grating based transverse electric (TE) pass polarizer using SOI platform is proposed and analyzed. The reported structure utilizes bi-metallic grating of noble metals; rhodium (Rh) and silver (Ag) as plasmonic materials to get benefit from their attractive properties. The rhodium is a corrosion-free, nonoxidizing, and chemically inert against aggressive chemicals noble metal. In conjunction with the use of Ag, Rh ensures better plasmonic response. The bi-metallic combination Ag/Rh exhibits large coupling between the quasi transverse magnetic mode confined in the silicon core and the surface plasmon mode constructed at the dielectric/metal interface, while the TE-mode can propagate with minimal losses. The modal characteristics of the proposed device are numerically investigated using full vectorial finite difference method, while the propagation analysis is performed using finite difference time domain method via Lumerical software package. The numerical results show that the TE-pass polarizer of a compact device length (L_D) = 3.5 μm offers an extinction ratio (ER) of 36.6 dB and an insertion loss (IL) of about 0.8 dB at $\lambda = 1.55 \mu\text{m}$. Additionally, the reported polarizer is robust to fabrication errors keeping the ER larger than 20 dB and the IL less than 1 dB despite changing the geometrical parameters by $\pm 10\%$ in the wavelength range of 1.4 to 1.7 μm .

Keywords Silicon photonics · Optical polarizers · Rhodium (Rh) · Hybrid plasmonic grating (HPG) · Polarization

1 Introduction

Photonic integrated circuits (PICs) (Dai et al. 2012) have recently become the most promising technology in designing high dense integrated chips since electronic integrated circuits have reached their maximum integration capacity. PICs exhibit attractive features such as, low thermal effects, large-scale integrated capacity, and high speed. In addition, a variety

✉ Mohamed Farhat O. Hameed
mfarahat@zewailcity.edu.eg

✉ S. S. A. Obayya
sobayya@zewailcity.edu.eg

Extended author information available on the last page of the article

of complex functions can be achieved using PICs with low-cost manufacturing processes. Silicon-on-insulator (SOI) technology is a prevailing platform that has been employed in designing both electronic and photonic components (Dai et al. 2012; Ye and Xiong 2013). The feature of SOI fabrication compatibility with mature CMOS technology permits integrating photonic and electronic devices on the same chip with high performance, low loss, and low cost. In SOI waveguides, the large index contrast between the silicon (Si) core and glass cladding (SiO_2 , Si_3N_4 , air, etc.) ensures strong light confinement enabling small device footprint. Further, SOI platform reduces parasitic capacitances that yield in improving the performance and reducing power consumption in the device. However, both geometrical birefringence and polarization dependence SOI devices are the two critical problems in SOI based nanophotonic waveguides and PICs. One solution is utilizing a polarization diversity scheme (Barwicz et al. 2007; Liu et al. 2011) where polarization controlling devices such as polarization splitters (Xu and Xiao 2016; Guan et al. 2014), polarization combiners and polarization rotators (Azzam et al. 2014a; Hameed et al. 2017a; Gao et al. 2013) have been presented to obtain polarization transparent PICs. However, a polarization diversity scheme, in which a beam of light is split at the input of the SOI chip and each polarization state is processed separately, is quite complex and increases the system size especially for simple applications. A polarizer can be used to pass the light wave of a specific polarization state through with minimal losses, while the other polarization state is highly suppressed. Because over half of the power is lost in single polarization systems, polarizers are obviously less efficient than polarization diversity systems. However, in devices that naturally rely on one polarization state, such as devices based on surface plasmons (Chen et al. 2008), a polarizer can be much simpler and more effective option. In this regard, a variety of optical polarizers have been proposed. All-dielectric optical polarizers (Dai et al. 2010; Saitoh et al. 2013; Wang and Ho 2010; Azzam et al. 2014b; Xu et al. 2020) have been introduced with minimal insertion losses (ILs) and high extinction ratios (ERs). However, the comparatively long device lengths, narrow bandwidths, and high sensitivity to fabrication errors of such structures are frequently a problem (Dai et al. 2010; Saitoh et al. 2013; Wang and Ho 2010; Azzam et al. 2014b; Xu et al. 2020).

Diffraction limit of light in dielectric media is a problem in which nanoscale regions far smaller than the wavelength of light are not supportive to electromagnetic waves localization in the material (Gramotnev and Bozhevolnyi 2010). Consequently, PICs may have considerable obstruction with miniaturization levels growth. On the other hand, plasmonic polarizers offer more compact and efficient designs because of its tendency to restrict light below the limit of diffraction (Sharma et al. 2011). However, high IL and fabrication difficulties limit the efficiency of plasmonic based devices. Metal-insulator-metal (MIM) designs (Ng et al. 2012; Huang et al. 2013) have been proposed with compact sizes and high ILs. In recent years, hybrid plasmonic waveguides (HPW) and hybrid plasmonic grating (HPG), or grating structures based on HPW have attracted a lot of interest for designing compact and highly efficient polarizers. In these structures, the two fundamental quasi-TE and -TM modes are guided in two different regions and by properly choosing the waveguide dimensions and material properties, their properties can be affected in different manners. In principle, HPW utilize the coupling between the dielectric/metal induced surface plasmon (SP) and one of the fundamental core-guided modes to eliminate the undesired mode. Thus, one of the polarization states propagates in a very confined manner with minimal losses, while the other one suffers high propagation loss. The coupling of dielectric/metal induced surface plasmon (SP) and one of the fundamental core-guided modes results in a supermode (Alam et al. 2011). This supermode, in case of the TE-pass polarizer, is mainly concentrated in the low index spacer region and in close vicinity of metal which

in turn attenuates the power of the fundamental quasi-TM mode in the hybrid guide. Further, in HPG-based structures, the plasmonic grating acts as a periodic perturbation for the effective refractive index of the medium in which this supermode propagates. Therefore, it will be highly reflected through N grating periods of the HPG section. Additionally, more SP modes are stimulated by the reflected light and more parts of energy is transferred to the SP modes from the reflected light (Bai et al. 2017). In this regard, an SOI-based hybrid plasmonic TM-pass polarizer has been reported with 18 μm device length (L_D) and an IL of more than 3 dB (Alam et al. 2011). However, this design which uses a silver layer as a metallic clade, has a CMOS incompatibility issue. Additionally, another TE-pass polarizer (Alam et al. 2012) that used chromium as a plasmonic material is proposed to serve compatibility with CMOS technology. Thus, it achieved a relatively high IL of 1 dB with along L_D of 17 μm . The experimental demonstration of the device reported in Alam et al. (2012) has been presented in Sun et al. (2012) showing an IL of 2–3 dB in the wavelength range of 1.52–1.58 μm with a very long L_D of 30 μm . Further, a CMOS compatible TE-pass polarizer has been fabricated with an $L_D=1$ μm , 16 dB ER and 2.2 dB IL in Huang et al. (2013). Furthermore, a compact 0.8 μm long TE-pass polarizer has been reported by Ying et al. in (2014) achieving an ER of 19 dB. Nevertheless, it is a CMOS incompatible device with a slightly high IL of 1 dB. Xu et al. (2016) have proposed a $\text{Ge}_2\text{Sb}_2\text{Te}_5$ (GST) based active TE- and TM- pass polarizers with ILs of 2.6 dB and 0.8 dB for the TE and TM pass polarizations, respectively with an $L_D=1$ μm . Additionally, ultracompact TE- and TM-pass polarizers have been reported in Abd-Elkader et al. (2019) based on aluminum doped zinc oxide (AZO). The 3.5 μm long TE-pass polarizer achieved ER of 20.6 dB and IL of 0.21 dB (Abd-Elkader et al. 2019). While, at an L_D of 1 μm , the TM-pass polarizer achieved an ER of 22 dB and an IL of 0.11 dB (Abd-Elkader et al. 2019). Moreover, Kandeel et al. (2019) have reported bi-metallic TE/TM-pass polarizers with an ER of 32.7 dB and 0.13 dB IL with an L_D of 1.5 μm . Another TM-pass polarizer has been proposed in Kandeel et al. (2019) with ER of 31.5 dB, IL of 0.17 dB and an L_D of 2 μm . In addition to the aforementioned devices in literature (Alam et al. 2011, 2012; Sun et al. 2012; Ying et al. 2014; Xu et al. 2016; Abd-Elkader et al. 2019; Kandeel et al. 2019), a variety of other hybrid plasmonic-based designs have been introduced in Azzam and Obayya (2015), Sun et al. (2016), Hameed et al. (2017b), Song and Xu (2018), Wu et al. (2020). Additionally, hybrid plasmonic grating (HPG) based structures have been proposed in Gaun et al. (2014), Zhang et al. (2014), Ni and Xiao (2019), Zafar et al. (2019), Wang et al. (2019), Hao et al. (2021), Xie et al. (2022). Further, Bai et al. (2017) have presented a compact HPG-based TM-pass polarizer that achieved an ER of 25 dB and IL of 0.088 dB at $L_D=2.5$ μm . However, the reported structure in Bai et al. (2017) is incompatible with CMOS technology. Another CMOS compatible multi-band TE-pass polarizer has been reported in Abadía et al. (2018) based on a HPG waveguide with a segmented metallic cladding. The polarizer can diffract the TM-mode and allow the propagation of the TE-mode achieving an ER of 20 dB and an IL of 1.7 dB with an L_D of 5.5 μm (Abadía et al. 2018). Moreover, a compact lithium niobate on insulator (LNOI) HPG TM-pass polarizer (Yu et al. 2019) with an L_D of 23 μm has been introduced with an ER of 20 dB and a relatively high IL of 2.5 dB. Bai et al. (2019) have experimentally presented a 6 μm -long HPG TE-pass polarizer with 24–33.7 dB ER and 2.8–4.9 dB IL in the wavelength range of 1.52 to 1.58 μm . Additionally, TiO_2 -based TM-pass polarizer (Zhao et al. 2020) has been introduced with ER of 27 dB and 2.64 μm long device. Another HPG TE-pass polarizer based on LNOI platform has been proposed by Dai et al. (2020) showing a 20 dB ER, and a relatively high IL of 2.3 dB with an L_D of 9 μm . It is worth mentioning that plasmonic waveguide-based polarizers suffer relatively low ERs, high ILs and fabrication difficulties using planar integrated technology. Although

HP waveguide-based structures have been introduced to enhance the performance, mostly obtained ILs are still unneglectable. Further, silver and gold, the conventional metals that are mostly used in hybrid plasmonic-based polarizers, are well-known with their incompatibility with current CMOS technologies.

In the growing field of nanoscale photonic devices, researchers have traditionally used many different plasmonic materials such as the noble metals (Ag and Au), copper (Cu), aluminum (Al) and chromium (Ch) due to their optimal plasmonic performance in visible and near-infrared (NIR) applications. Despite of the superior plasmonic response of Ag, chemical instability, and oxide formation upon exposure to air limit its effectiveness. While Au agglomerates and can't be formed in a thin uniform film, copper, aluminum, and chromium are affected by oxidization which tarnishes its performance upon exposure to air.

Rhodium (Rh) is a silvery-white, corrosion free, chemically inert and is not attacked by most acids noble metal (Homola et al. 1999). It is rarely used in plasmonic applications because it is a heavily lossy metal that can't be utilized in bulk. However, high absolute value of its permittivity real part may promise to be very fruitful for plasmonic applications when using a very thin layer of it (Kurihara and Suzuki 2002). Recently, theoretical studies have proved that fabrication of Rh nanoparticles smaller than 10 nm is possible (Zetsu et al. 2006). Moreover, Rh is routinely used in a wide variety of applications (Shelef and Graham 1994; Goto et al. 2014). Rhodium is routinely added to platinum (Pt) and palladium (Pd) alloys to make them harder and lose weight much slower than pure platinum at high temperature. Such alloys usage is dominated in the three-way catalytic converters to reduce nitrogen oxide in exhaust emissions. In the chemical industry, rhodium is also used as a catalytic agent for nitric acid production and hydrogenation reactions of organic compounds. Its high reflectivity for light (Coblentz and Stair 1939), makes Rh a good candidate for reflecting surfaces in optical instruments. Rhodium is a non-oxidizing that doesn't normally form oxides even when heated and has a high melting point that can't be tarnished by the atmosphere at room temperature (Ahmadivand et al. 2016). So, it is usually plated onto white gold to improve its appearance and silver is frequently plated by a thin layer of rhodium to resist tarnishes. Rh has proved to be a viable candidate for plasmonic based sensing applications (Ahmadivand et al. 2016; Mishra and Mishra 2016; Mishra et al. 2020) because of the high real part of its permittivity. On the other side, Rh has not very sharp resonance feature due to the high imaginary part of its permittivity that causes non-negligible material losses. Therefore, a very thin Rh layer is considered in collaboration with an Ag layer in different sensing applications to enhance the resonance sharpness. A bi-metallic layer of Rh/Ag based Magnesium Fluoride (MgF_2) prism-coupled gas sensor in the visible region has been proposed in Mishra and Mishra (2016). Furthermore, another aqueous samples highly sensitive sensing probe based on bimetallic plasmonic of Rh/Ag in the visible region has been presented in Mishra et al. (2020).

In this paper, a bi-metallic (Rhodium–Silver) grating structure based on SOI platform is used in designing a compact TE-pass polarizer. By optimally choosing the geometrical parameters, the TM mode is highly attenuated by the plasmonic grating, while the TE mode passes through the dielectric core with low loss. Full vectorial finite difference method (FVFD) is employed to perform the modal analysis of the proposed polarizer. Furthermore, the 3D finite difference time domain (3D-FDTD) method (www.lumerical.com/tcadproducts/fdtd/e) is utilized to investigate the propagation characteristics of the proposed structure. The simulation results indicate that the proposed polarizer achieves 36.6 dB ER and about 0.8 dB IL with L_D of 3.5 μm . Thus, the reported HPG polarizer exhibits higher ER than the previously reported in Dai et al. (2010), Wang and Ho (2010), Azzam et al. (2014b), Xu et al. (2020), Sharma et al. (2011), Ng et al. (2012), Huang et al.

(2013), Ying et al. (2014), Abd-Elkader et al. (2019), Kandeel et al. (2019), Azzam and Obayya (2015), Sun et al. (2016), Hameed et al. (2017b), Song and Xu (2018), Wu et al. (2020), Gaun et al. (2014), Zhang et al. (2014), Zafar et al. (2019), Wang et al. (2019), Hao et al. (2021), Bai et al. (2017), Abadía et al. (2018), Yu et al. (2019), Bai et al. (2019), Zhao et al. (2020), Dai et al. (2020) and lower IL than those of the previously demonstrated HP polarizers based on SOI (Huang et al. 2013; Alam et al. 2011, 2012; Sun et al. 2012; Ying et al. 2014; Xu et al. 2016; Gaun et al. 2014; Zhang et al. 2014; Wang et al. 2019; Abadía et al. 2018; Bai et al. 2019) and those based on LNOI platform (Yu et al. 2019; Dai et al. 2020).

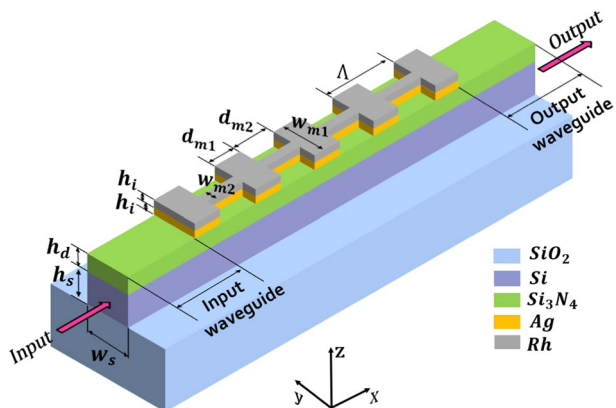
2 Design consideration

The proposed device consists of a HPG structure in which the polarizer section is sandwiched between two identical input and output single mode Si waveguides as may be seen in the 3D view depicted in Fig. 1. The proposed HPG polarizer consists of a high-index Si core that is separated from a bi-metallic grating of noble metals (Ag and Rh) through a low-index spacer of silicon nitride (Si_3N_4). The reported design is based on the well-known SOI platform where the refractive indices of Si, SiO_2 , Si_3N_4 , Ag, and Rh at $\lambda = 1.55 \mu\text{m}$ are 1.46, 3.48, 2.17 (Steinlechner et al. 2017), $0.145 + 11.438i$ (Johnson and Christy 1972), and $3.63 + 10.3i$ (Adachi 2012), respectively. To design a TE-pass polarizer, the quasi-TE mode should be well-confined in the core region with very small propagation loss, while the quasi-TM mode should suffer high propagation loss.

As may be seen in Fig. 1, the bi-metallic grating is set in the vertical direction (z-axis) to enhance the coupling between the surface plasmon mode (SPM) guided by the Si_3N_4 /bi-metallic interface and quasi-TM mode supported by the Si core. In contrast, the quasi-TE mode is well confined in the Si core throughout the whole propagation length.

The input and output waveguides are standard low-loss single mode Si waveguides ($h_s = 220 \text{ nm}$ and $w_s = 500 \text{ nm}$) to couple the light smoothly in and out from the HPG section. The spacer has the same width w_s of the Si core with a different height of h_d . The bi-metallic grating width alters periodically between w_{m1} and w_{m2} , with depths of d_{m1} and d_{m2} , respectively and a thickness of h_i for each plasmonic layer, as may be seen in Fig. 1.

Fig. 1 3D schematic configuration of the proposed SOI based TE-pass polarizer



3 Analysis and numerical results

The modal analysis of the proposed HPG waveguide is performed using the full-vectorial finite difference method (FVFD) via Lumerical software package (www.lumerical.com/tcadproducts/fdtd/e). It is worth mentioning that a perfectly matched layer (PML) boundary conditions and grid size of $\Delta y = \Delta z = 0.005 \mu\text{m}$, and $\Delta x = 0.03 \mu\text{m}$ are applied in this study. Figure 2 shows how the conventional 220 nm thick Si waveguide deals with different polarizations of light at $\lambda = 1.55 \mu\text{m}$. For the TE-polarized light, most of the electric field intensity is concentrated in the core region. However, the TM-polarized one has large leakage outside the Si core. Therefore, the quasi-TM mode can make strong coupling with the SPM unlike the quasi-TE polarized mode. Therefore, by adding the plasmonic layers, the TM-polarized light will be strongly attenuated because of the strong power coupling with the SPM as may be seen in Fig. 2d. In contrast, the quasi-TE mode is still confined in the Si core even after adding the plasmonic layers, Fig. 2b. It is worth mentioning that in Fig. 2b, d, the HPWG has a 140 nm thick spacer of SiO_2 followed by bimetallic plasmonic layer of Ag/Rh with $h_i = 10 \text{ nm}$ and $w_{m1} = 500 \text{ nm}$.

To study the effect of the structure geometrical parameters on the coupling between the two modes supported by the input DW and HPWG, coupling coefficient (the reflection intensity per unit length) calculated by $(k = 2\Delta n_{\text{eff}} / (n_{\text{eff}}\Lambda))$ (Bai et al. 2017) is considered, where n_{eff} , Δn_{eff} and Λ are the mode effective index, mode effective index difference ($n_{\text{eff_HPW}} - n_{\text{eff_DW}}$), and grating period, respectively. Accordingly, to prevent high loss for the TE mode, Δn_{eff} (TE) must be as small as possible. However, the

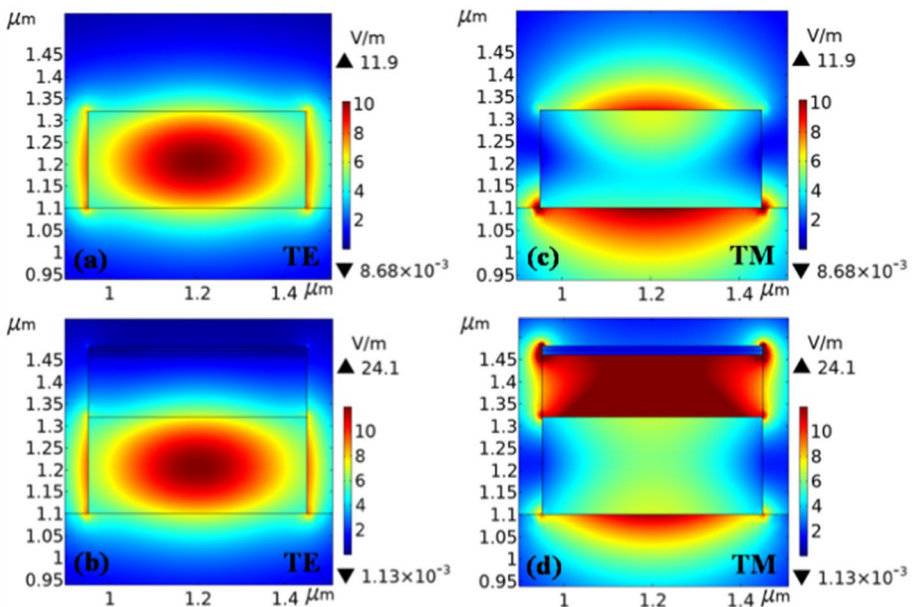


Fig. 2 Normalized electric field plots of **a** the quasi-TE mode, and **c** the quasi-TM mode, of the dielectric waveguide (DW) at $\lambda = 1.55 \mu\text{m}$, **b** the quasi-TE mode, and **d** the quasi-TM mode, of the HPWG at $\lambda = 1.55 \mu\text{m}$. Here, a 140 nm thick layer of SiO_2 and Ag/Rh bi-metallic structure of $h_i = 10 \text{ nm}$ and $w_{m1} = 500 \text{ nm}$ is used

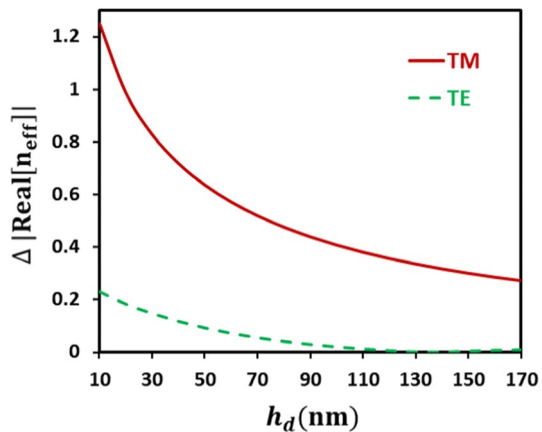
TM-mode should have large Δn_{eff} . To further clarify this concept, the impact of changing the spacer thickness (h_d) on the amount of reflection intensity is studied for both polarizations. It is worth mentioning that the spacer layer is initially assumed to be silica (SiO_2). The absolute value of real Δn_{eff} , the difference of the real parts of the effective indices correspond to the quasi-TE and quasi-TM modes of the DW and HPW, for the two polarizations is calculated as function of h_d , considering a plasmonic layer of Rh for the HPWG with $h_i = 10$ nm and $w_{m1} = 500$ nm and the results are depicted in Fig. 3.

As it may be seen in Fig. 3, Δn_{eff} for quasi-TM mode increases distinctly by reducing the SiO_2 thickness. Thus, it is expected that the quasi-TM mode will suffer high coupling losses towards the plasmonic grating over several periods at small values of h_d . However, for the quasi-TE mode, although Δn_{eff} decreases slowly by increasing the spacer thickness, it is relatively insensitive to h_d variations especially over the range $h_d = 120$ – 170 nm. For a good TE-pass polarizer, the TE-polarized light should propagate throughout the whole device with very low losses. Thus, $h_d = 140$ nm is an optimum value at which $|\Delta \text{Real}[n_{\text{eff}}]|$ for the quasi-TE mode is 0.0018, while it is 0.3 for the quasi-TM mode as revealed by Fig. 3. When the TM polarized light is launched from the input DW, the quasi-TM mode will be highly reflected through N grating periods of the HPG section. However, the launched TE-polarized light will be almost unaffected. The thickness of the metal layers also influences the polarizer's performance as shown in Fig. 4, where h_d and w_{m1} are fixed to 140 nm and 500 nm, respectively.

First, the case of using a single layer of Rh is studied to distinguish its impact on the propagation of the two polarizations. Figure 4a shows that the quasi-TM mode coupling becomes stronger when the thickness of Rh layer is less than 20 nm. However, the quasi-TE mode is almost unaffected by h_i variations. Additionally, the same results are obtained for an Ag layer instead of Rh as shown in Fig. 4b. So, $h_i = 10$ nm is the most suitable option to achieve strong coupling for the quasi-TM-mode alongside fitting manufacturing requirements limitations.

The well-known FDTD method via Lumerical software package (www.lumerical.com/tcadproducts/fdtd/e) is utilized to perform the 3D simulations to investigate the propagation characteristics of the proposed TE-pass polarizer. In this study, the ER and IL are calculated from Eqs. (1)–(3).

Fig. 3 The calculated difference of the real parts of the effective indices correspond to the quasi-TE and quasi-TM modes of the DW and HPW as a function of the SiO_2 spacer thickness, using single Rh plasmonic layer of $h_i = 10$ nm and $w_{m1} = 500$ nm at $\lambda = 1.55$ μm



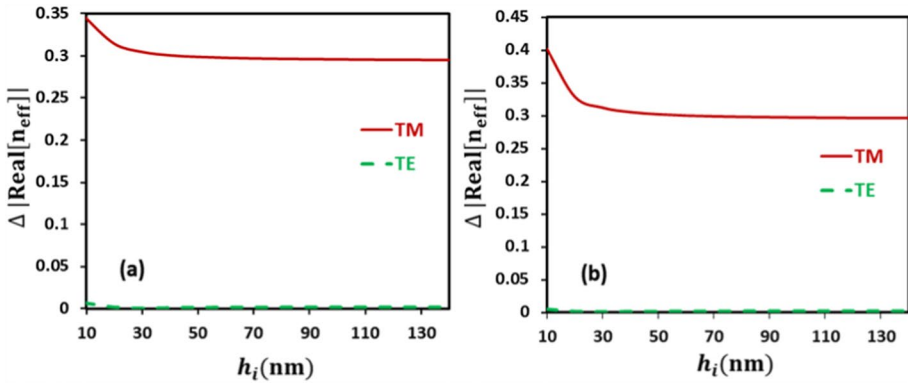


Fig. 4 The calculated difference of the real parts of the effective indices correspond to the quasi-TE and quasi-TM modes of the DW and HPW when the plasmonic material is a single layer of **a** Rh, and **b** Ag as a function of the metallic layer thickness (h_i) while $w_{m1} = 500$ nm and h_d is fixed to 140 nm at $\lambda = 1.55$ μ m

$$ER(\text{dB}) = 10 \log_{10} \left(\frac{P_{TE}^{out}}{P_{TE}^{in}} \times \frac{P_{TM}^{in}}{P_{TM}^{out}} \right) \tag{1}$$

$$IL_{TE}(\text{dB}) = 10 \log_{10} \left(\frac{P_{TE}^{out}}{P_{TE}^{in}} \right) \tag{2}$$

$$IL_{TM}(\text{dB}) = 10 \log_{10} \left(\frac{P_{TM}^{out}}{P_{TM}^{in}} \right) \tag{3}$$

where P_{TE}^{out} and P_{TE}^{in} are the powers of the quasi-TE mode at the output and input ports of the polarizer, respectively. Further, P_{TM}^{out} and P_{TM}^{in} are the powers of the undesired quasi-TM-mode at the output and input ports of the polarizer, respectively.

For high performance TE-pass polarizer, a very high ER and low IL_{TE} should be achieved. Thus, the grating duty cycle (η)= d_{m1}/Λ , should be properly chosen to enlarge the quasi-TM mode reflection and insignificantly affect the quasi-TE mode propagation process. In this study, the cases of $\eta = 0.5, 0.6$ and 0.7 are studied in detail. Since the spacer and plasmonic grating material properties are very influential to be considered, a detailed numerical study is also carried out to investigate material properties of the spacer and plasmonic gratings at which the highest ER and the lowest IL_{TE} are possible.

The effect of variation in d_{m1} on the proposed TE-pass polarizer’s performance is studied in terms of ER and IL. First, the case of $w_{m2} = 0$ is studied with $w_{m1} = 500$ nm, $h_i = 10$ nm and number of periods (N)= 5 where the SiO_2 spacer thickness is fixed to 140 nm. In this study, single metallic grating of Ag and Rh are investigated. Further, the bi-metallic grating of Ag/Rh is considered where the Ag is the lower grating. As it should be noticed from Fig. 5a–f, Ag plasmonic grating mostly acquires the best ER values with the lowest IL_{TE} . However, for the same circumstances but using a 140 nm thick Si_3N_4 spacer (instead of SiO_2), Rh plasmonic grating can exhibit better results. In this context, the obtained ER in case of using a single metallic grating of Rh surpasses that of Ag in more than one place especially at large values of duty cycle as may be seen in Fig. 6a–c. It is worth

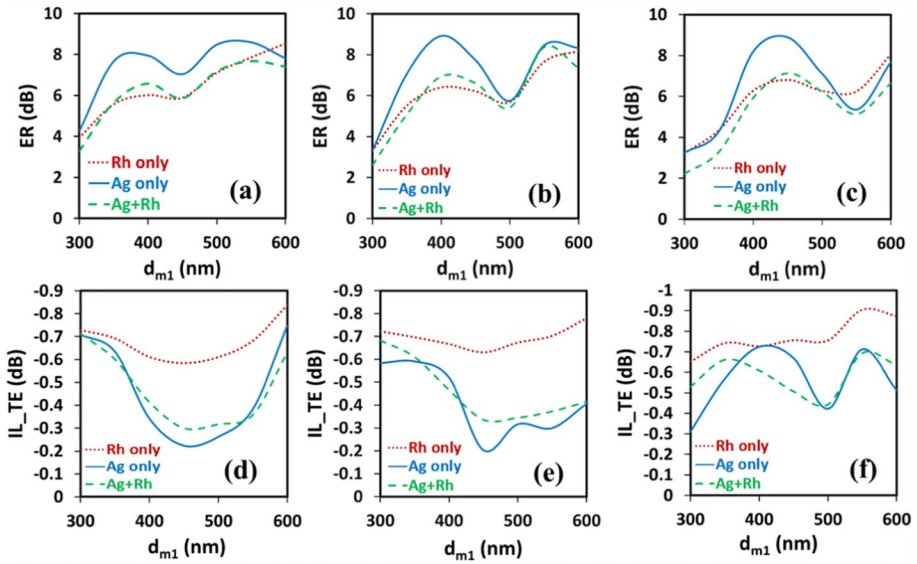


Fig. 5 Variation of **a–c** extinction ratio (ER) and **d–f** insertion loss (IL_{TE}) with the metallic depth d_{m1} using different plasmonic materials and different duty cycles **a, d** $\eta=0.5$, **b, e** $\eta=0.6$, and **c, f** $\eta=0.7$ with a 140 nm thick SiO_2 spacer, $w_{m1}=500$ nm, $w_{m2}=0$, $hi=10$ nm and $N=5$

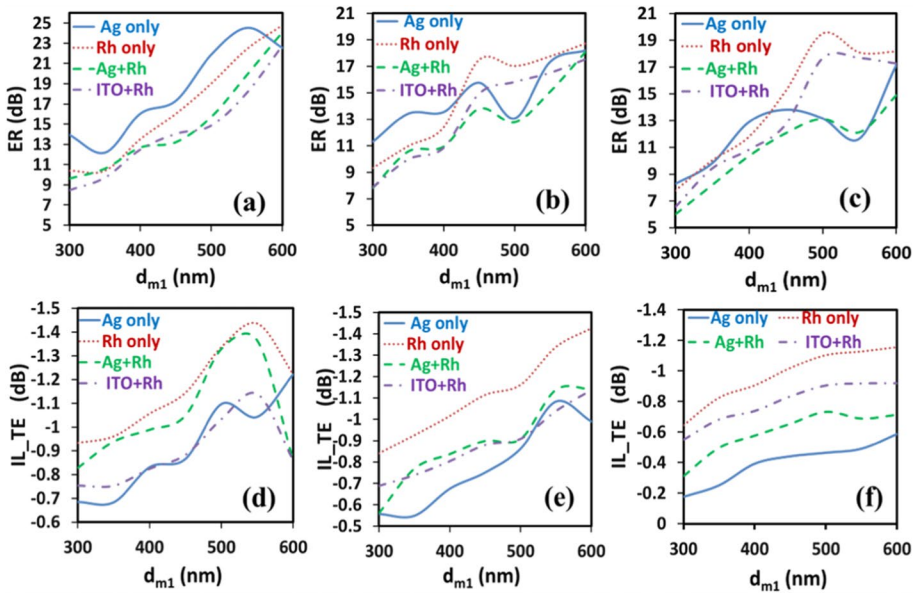


Fig. 6 Variation of **a–c** ER and **d–f** IL_{TE} with the metallic depth d_{m1} using different plasmonic materials and different duty cycles **a, d** $\eta=0.5$, **b, e** $\eta=0.6$, and **c, f** $\eta=0.7$ with a 140 nm thick Si_3N_4 spacer, $w_{m1}=500$ nm, $w_{m2}=0$, $hi=10$ nm and $N=5$

mentioning that $h_i = 10$ nm, $N = 5$ and a Si_3N_4 spacer of 140 nm are considered for subsequent simulations.

Using bi-metallic structures is expected to enhance the operation of the proposed polarizer in terms of ER. Indium tin oxide (ITO) is one of the transparent conducting oxides (TCOs) that also can replace the conventional plasmonic materials owing to their unique properties such as design flexibility, compatibility with CMOS fabrication technology, epsilon-near-zero (ENZ) effect in the near infrared and electrically tunable permittivity (Babicheva et al. 2015). Thus, ITO has been widely employed in different passive and active devices. The feature of tunable optical properties of ITO depends on modifying its carrier concentration by heavily doping, electrical gating, or post deposition rapid thermal annealing processes. This feature allows a flexible tuning to ITO's complex refractive indices that are linked to the carrier concentration (Lee et al. 2014; Capretti et al. 2015). At low carrier concentration, ITO has a dielectric-like optical property with low absorption. However, the high concentration of carriers in ITO significantly affects its permittivity.

Within our investigations, the tunable permittivity of ITO material and the operating condition of its ENZ effect are also tested. The tunable permittivity of ITO can be described by Drude model (Huang 2016) with different carrier concentrations as,

$$\varepsilon(\omega) = \varepsilon_\infty - \frac{\omega_p^2}{\omega(\omega + i\gamma)}, \quad \omega_p^2 = \frac{ne^2}{\varepsilon_0 m^*} \quad (4)$$

where ε_∞ is the high frequency permittivity, ω is the angular frequency, ω_p is the plasma frequency, γ is the electron scattering rate, $m^* = 0.35 m_0$ is the effective mass ($m_0 = 9.1 \times 10^{-31}$ kg is the rest mass of electron), n is the carrier concentration of ITO under different doping level, and e is the electron charge. For ITO, $\varepsilon_\infty = 3.9$, $\gamma = 1.8 \times 10^{14}$ rad/s, and with a certain electron concentration ($\sim 6.47 \times 10^{20} \text{ cm}^{-3}$). It is worth mentioning that the real part of ITO permittivity approaches zero at the wavelength of 1.55 μm , while the corresponding imaginary part increases to ~ 0.5774 (Huang 2016) producing high absorption loss. In this context, a bi-metallic grating of a 10 nm thick Ag layer and 10 nm thick Rh layer and another bi-metallic grating of 10 nm ITO and 10 nm Rh layers are tested, and the results are shown in Fig. 6.

It may be seen from Fig. 6a that with a duty cycle of 0.5 and $d_{m1} = 600$ nm, the obtained ER of using a single Rh grating is 24.79 dB. However, ERs of about 22.6 dB, 24.1 dB, and 22.8 dB are obtained when using single Ag grating, bi-metallic grating of Ag/Rh, and bi-metallic grating of ITO/Rh, respectively. For duty cycles of 0.6 and 0.7, single Rh grating could achieve better ER than that of the bi-metallic grating of Ag/Rh and the bi-metallic grating of ITO/Rh along all the d_{m1} range, Fig. 6b, c. Additionally, the single Rh grating could obtain higher ER values than that of the single 10 nm thick Ag grating after $d_{m1} = 450$ nm range, Fig. 6c. Furthermore, the bi-metallic grating of ITO/Rh could exhibit a preferable ER that is compared to that of single Ag grating, i.e., at $\eta = 0.7$ and $d_{m1} = 550$ nm, Fig. 6c. The obtained ER in case of using bi-metallic grating of ITO/Rh is higher than 17.5 dB, while that of the single Ag grating is less than 12 dB with the same duty cycle. Figure 6d–f show the effect of the depth (d_{m1}) of the plasmonic gratings on IL_{TE} mode using different plasmonic materials and different duty cycles. It is also evident that Ag plasmonic grating offers the lowest IL_{TE} along most of the studied d_{m1} range when $\eta = 0.5$ and 0.6 and along the whole studied d_{m1} range when $\eta = 0.7$. However, bi-metallic grating of ITO/Rh achieves much lower IL than that of Ag grating at $\eta = 0.6$ when $d_{m1} = 550$ nm. As it is shown in Fig. 6e, when d_{m1} is fixed to 550 nm, the IL in case of using Ag grating is -1.08 dB, but for the bi-metallic grating of ITO/Rh it is about -1.04 dB. Moreover, at

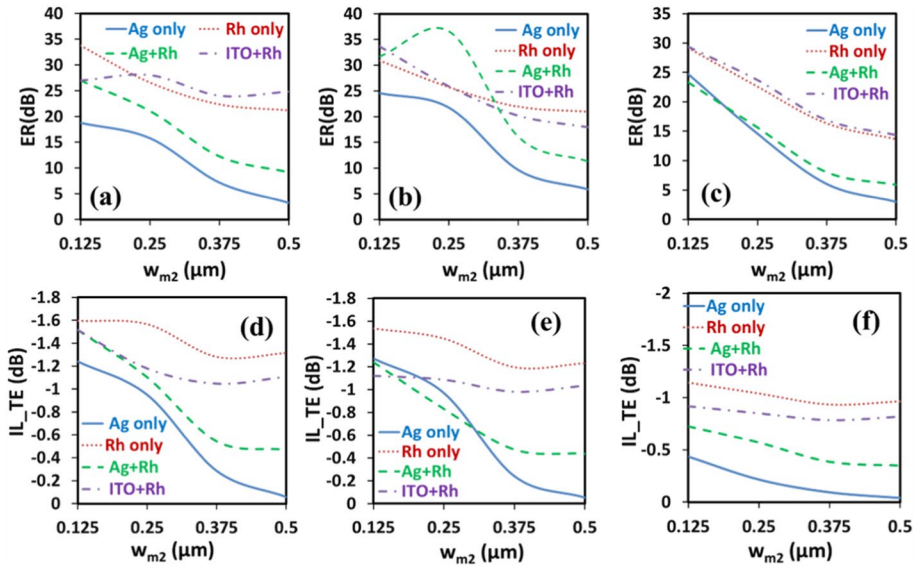


Fig. 7 Variation of **a–c** ER and **d–f** IL_{TE} with the metallic width w_{m2} using different plasmonic materials and different duty cycles **a, d** $\eta=0.5$ and $d_{m1}=500$ nm, **b, e** $\eta=0.6$ and $d_{m1}=550$ nm, **c, f** $\eta=0.7$ and $d_{m1}=500$ nm, with a 140 nm thick Si_3N_4 spacer, $w_{m1}=500$ nm, $hi=10$ nm and $N=5$. It is worth noting that the case of HPW is attained with $w_{m2}=0.5$ μm

$\eta=0.5$ and $d_{m1}=600$ nm, about -0.86 dB IL is obtained in the two studied cases of the bi-metallic grating (Ag/Rh and ITO/Rh) and an IL of -1.2 dB is achieved when using single grating (Ag or Rh), Fig. 6d.

On the other hand, another investigation is performed for the case of $w_{m2} \neq 0$. The impact of the variation in w_{m2} on the proposed TE-pass polarizer's performance is studied in terms of ER and IL. Considering $N=5$, Si_3N_4 thickness of 140 nm and $w_{m1}=500$ nm, the cases of $d_{m1}=500$ nm at $\eta=0.5$, $d_{m1}=550$ nm at $\eta=0.6$ and $d_{m1}=500$ nm at $\eta=0.7$ are studied and the results are shown in Fig. 7.

As it may be seen in Fig. 7a, c, both single Rh grating and ITO/Rh bi-metallic grating possess the highest ER over the whole considered range of w_{m2} especially at $w_{m2}=0.125$ μm . When $\eta=0.5$ and $w_{m2}=0.125$ μm , ERs of 33.7 dB and 27 dB are achieved when using single Rh grating and ITO/Rh bi-metallic grating, respectively as shown in Fig. 7a. Additionally, ERs of about 29.2 dB, and about 29.4 dB are obtained when using single Rh grating and the ITO/Rh bi-metallic grating at $\eta=0.7$ and $w_{m2}=0.125$ μm , respectively, Fig. 7c. However, it should be noted from Fig. 7b that at $\eta=0.6$ and $w_{m2}=0.25$ μm , the bi-metallic grating of Ag/Rh achieves the highest ER of 36.6 dB superior to those of the reported polarizers introduced in mentioned (Dai et al. 2010, 2020; Wang and Ho 2010; Azzam et al. 2014b; Xu et al. 2020; Sharma et al. 2011; Ng et al. 2012; Huang et al. 2013; Ying et al. 2014; Abd-Elkader et al. 2019; Kandeel et al. 2019; Azzam and Obayya 2015; Sun et al. 2016; Hameed et al. 2017b; Song and Xu 2018; Wu et al. 2020; Gaun et al. 2014; Zhang et al. 2014; Zafar et al. 2019; Wang et al. 2019; Hao et al. 2021; Bai et al. 2017, 2019; Abadía et al. 2018; Yu et al. 2019; Zhao et al. 2020).

Figure 7d–f depict the variations of the width (w_{m2}) of the plasmonic gratings and the induced effect on IL using different plasmonic materials and different duty cycles. It is evident from Fig. 7d–f that in case of single Ag grating or bi-metallic grating of Ag/Rh, the

Table 1 The optimal dimensions for the proposed quasi-TE pass polarizer

Dimension	w_s (nm)	h_s (nm)	h_d (nm)	w_{m1} (μm)	w_{m2} (μm)	h_i (for Ag) (nm)	h_i (for Rh) (nm)	d_{m1} (nm)	η
Value	500	220	140	0.5	0.25	10	10	550	0.6

IL decreases with the increment of w_{m2} . Additionally, using the bi-metallic grating of Ag/Rh, IL of about $- 0.8$ dB is obtained when $\eta=0.6$ and $w_{m2}= 0.25 \mu\text{m}$, as shown in Fig. 7e. Furthermore, single Rh grating and bi-metallic grating of ITO/Rh achieve their lowest IL values (about $- 0.9$ dB and about $- 0.8$ dB), respectively, at $\eta=0.7$ and $w_{m2} = 0.375 \mu\text{m}$, as shown in Fig. 7f. It is worth mentioning that at $w_{m1}=w_{m2}=0.5 \mu\text{m}$, the proposed design acts as an HPW that achieves ER of 11.3 dB and IL of 0.4 dB, as shown in Fig. 7b, e, respectively. Although the HPG design results in 0.8 dB which is more than that obtained by similar HPW, the 0.8 dB is still in the acceptable range (less than 1 dB). However, the ER of the HPG-based structure (36.6 dB) is much higher than that of the HPW. It is worth noting that Table 1 depicts the optimum dimensions of the presented HPG polarizer while Table 2 provides a comparison between the dimensions used for the proposed HPG and HPW designs and obtained results.

The effect of the variation in plasmonic grating width (w_{m1}) on the ER and IL of the quasi-TE pass polarizer is then investigated. Firstly, the case of $w_{m2} = 0$, $d_{m1} = 600$ nm and using Rh single plasmonic grating at $\eta=0.5$ is considered and the obtained results are shown in Fig. 8a. It may be noted from Fig. 8a that ER curve reaches its highest value of about 27.1 dB with $- 1.03$ dB IL at $w_{m1} = 0.4 \mu\text{m}$. However, the lowest IL of $- 0.2$ dB is obtained with an ER of 16.4 dB at $w_{m1}= 0.1 \mu\text{m}$ and an L_D of $4.4 \mu\text{m}$. Further, the case of $w_{m2}= 0.25 \mu\text{m}$, $d_{m1}= 550$ nm when using bi-metallic gratings of Ag/Rh at $\eta=0.6$ is also considered and the obtained results are shown in Fig. 8b. As it can be observed from

Table 2 Comparison between the proposed HPG and HPW designs in terms of dimensions and obtained ER and IL, reflection and transmission coefficients

Design		HPG	HPW
Dimensions	h_d	140 nm	140 nm
	h_i	10 nm	10 nm
	w_{m1}	$0.5 \mu\text{m}$	$0.5 \mu\text{m}$
	w_{m2}	$0.25 \mu\text{m}$	$0.5 \mu\text{m}$
	η	0.6	-
	d_{m1}	550 nm	-
	N	5	-
	Device length	$3.5 \mu\text{m}$	$3.5 \mu\text{m}$
Obtained ER	-	36.6 dB	11.3 dB
Obtained IL	-	0.8 dB	0.4 dB
Reflection coefficient	Quasi-TE mode	0.0057 ($- 22.4$ dB)	0.0046 ($- 23.4$ dB)
	Quasi-TM mode	0.035 ($- 14.6$ dB)	0.0033 ($- 24.8$ dB)
Transmission coefficient	Quasi-TE mode	0.83 ($- 0.81$ dB)	0.9 ($- 0.46$ dB)
	Quasi-TM mode	0.00018 ($- 37.4$ dB)	0.067 ($- 11.74$ dB)

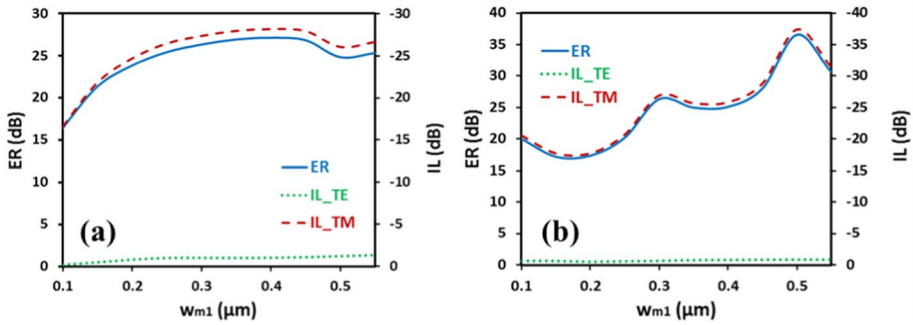


Fig. 8 Extinction ratio (ER) and Insertion loss (IL) variations of the quasi-TE pass polarizer with the metallic width w_{m1} using a spacer layer of 140 nm thick Si_3N_4 , $h_i=10$ nm and $N=5$ in case of **a** 0.5 duty cycle, $d_{m1}=600$ and $w_{m2}=0$, using Rh single plasmonic grating and **b** 0.6 duty cycle, $d_{m1}=550$ and $w_{m2}=0.25$ μm , using Ag/Rh bi-metallic grating

Fig. 8b, at $w_{m1} = 0.5$ μm , an ER of 36.6 dB and an IL of -0.8 dB are obtained at a dense length of 3.2 μm . Further, the metallic width (w_{m1}) variations have a slight effect on IL results. It is worth mentioning that the IL values lie between -0.6 dB and -0.8 dB with the w_{m1} variations from 0.1 to 0.55 μm are obtained.

In this study, as a trade-off between the obtained ER and IL results, using Si_3N_4 layer as a spacer and Ag/Rh bi-metallic grating, a compact L_D of 3.2 μm is chosen that offers an ER of 36.6 dB and IL of about -0.8 dB while utilizing the geometrical dimensions depicted in Table 1.

The fabrication tolerance of different geometrical parameters of the proposed polarizer has also been investigated. In this study, the effect of varying the thickness of the Si_3N_4 spacer layer (h_d), the thickness and the widths of the Ag/Rh bi-metallic grating (h_i), (w_{m1} , w_{m2}), respectively, by ± 10 nm around their optimal values is studied. Table 3 depicts the obtained ER and IL of the reported device according to these variations. It can be noted from Table 3 that some geometrical parameters have stronger impact on the performance of the quasi-TE-pass polarizer than others. However, the reported polarizer achieves acceptable performance, where ER is always better than 20 dB with IL less than 1 dB. Moreover, the quasi-TE pass polarizer offers an ER which is better than 27 dB with $\text{IL} \leq 1$ dB when the thickness (h_i) of both Ag and Rh gratings is varied

Table 3 Calculated ER and IL due to fabrication tolerance of $\pm 10\%$ for different geometrical parameters of the proposed quasi-TE pass polarizer

Geometrical parameter (nm)	ER (dB)	IL (dB)
$h_d + 10\%$	20.9	0.7
$h_d - 10\%$	21	1
$h_i + 10\%$ (for Ag thickness)	27.4	0.7
$h_i - 10\%$ (for Ag thickness)	27.5	0.96
$h_i + 10\%$ (for Rh thickness)	36.9	0.8
$h_i - 10\%$ (for Rh thickness)	27.5	0.96
$w_{m1} + 10\%$	30.6	0.8
$w_{m1} - 10\%$	28	0.8
$w_{m2} + 10\%$	28.9	0.7
$w_{m2} - 10\%$	31.7	0.97

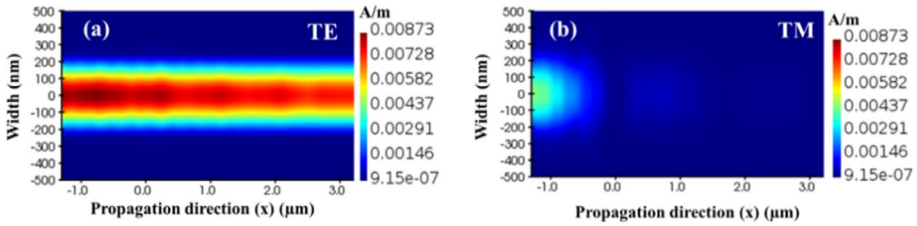
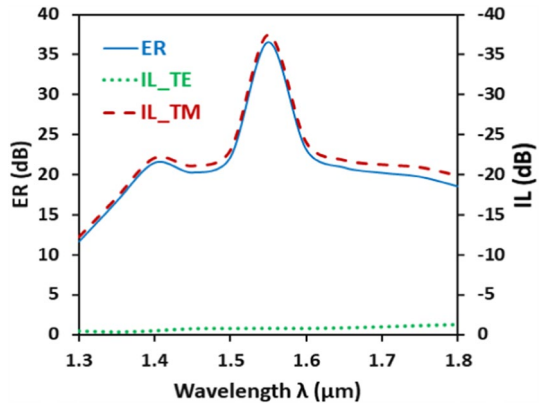


Fig. 9 Light propagation through the suggested TE-pass polarizer excited by **a** TE polarized mode and **b** TM polarized mode. Here, a 140 nm thick layer of Si_3N_4 and Ag/Rh bi-metallic structure of $h_i = 10$ nm, $w_{m1} = 500$ nm, $w_{m2} = 250$ nm and $N = 5$ are used in case of $d_{m1} = 550$ nm and $\eta = 0.6$

Fig. 10 Extinction ratio (ER) and Insertion loss (IL) variations of the quasi-TE pass polarizer with the wavelength. Here, a 140 nm thick layer of Si_3N_4 and Ag/Rh bi-metallic structure of $h_i = 10$ nm, $w_{m1} = 500$ nm, $w_{m2} = 250$ nm and $N = 5$ are used in case of $d_{m1} = 550$ nm and $\eta = 0.6$



by ± 10 nm around their optimal values. Further, an ER values that are ≥ 28 dB with $IL < 1$ dB are achieved when varying the widths (w_{m1}, w_{m2}) of the Ag/Rh bi-metallic grating by ± 10 nm around their optimal values. Thus, it is revealed that the reported quasi-TE pass polarizer has good robustness to fabrication imperfections.

To investigate the propagation characteristics of the reported quasi-TE pass polarizer, 3D FDTD simulations are performed via Lumerical software package (www.lumerical.com/tcadproducts/fdtd/e) with mesh size of $\Delta y = \Delta z = 0.005 \mu\text{m}$, and $\Delta x = 0.03 \mu\text{m}$. Figure 9 shows the propagation of the light through the proposed polarizer when excited with quasi-TE and TM modes using the structural parameters mentioned in Table 1. As it can be seen from Fig. 9a, the input TE mode is well-propagated through the polarizer section with low losses. However, the input quasi-TM mode is a highly attenuated due to the coupling with the SP mode, as shown in Fig. 9b.

The operating bandwidth of the reported TE-pass polarizer is also investigated where the wavelength-dependent ER and IL variations are calculated as shown in Fig. 10. The results show that the presented TE-pass polarizer offers relatively broad bandwidth of operation. It is revealed from Fig. 10 that the proposed TE-pass polarizer achieves $ER > 20$ dB and $IL < 1$ dB through the wavelength range of 1.4–1.7 μm with bandwidth of 300 nm. It may be also noted from Fig. 10 that ER curve reaches its highest value of about 36.6 dB with 0.8 dB IL at $\lambda = 1.55 \mu\text{m}$. However, through the wavelength range before $\lambda = 1.4 \mu\text{m}$ and after $\lambda = 1.7 \mu\text{m}$, the ER curve drops to < 20 dB. Additionally, the IL of the reported TE-pass polarizer achieves values < 1 dB through the wavelength

range of 1.3–1.7 μm , however, it exceeds 1 dB after $\lambda = 1.7 \mu\text{m}$. Therefore, the wavelength has a good tolerance of $1.55 \mu\text{m} \pm 0.15 \mu\text{m}$ where the $\text{ER} > 20 \text{ dB}$ and $\text{IL} < 1 \text{ dB}$.

The wavelength dependence reflection of the proposed TE-pass polarizer is also investigated through the wavelength range of 1.4–1.7 μm . Figure 11 shows the variation of the reflection losses of the quasi-TE and quasi-TM modes of the reported design with the wavelength. In this study, the reflection loss is given by:

$$\text{Reflection loss} = 10 \log_{10} \left(\frac{P_r}{P_i} \right) \quad (5)$$

where P_r is the reflected power and P_i is the input power. It may be seen from Fig. 11 that the reflection is unavoidable for both the quasi-TE mode and the quasi-TM mode. However, the reflection of the quasi-TM mode is higher than that of the quasi-TE mode through the wavelength range of 1.4–1.6 μm . It is also evident from Figs. 10 and 11 that at $\lambda = 1.55 \mu\text{m}$, the obtained ER of the proposed polarizer is 36.6 dB while the calculated reflection losses for the quasi-TE and quasi-TM modes are -22.4 dB and -14.5 dB , respectively. Thus, the quasi-TE mode has smaller reflection loss than that of the quasi-TM mode which enhances the operation of the proposed TE pass polarizer in terms of ER. Further, the quasi-TE mode has a reflection coefficient of 0.0057 (-22.4 dB) and transmission coefficient of 0.83 (-0.81 dB). However, the quasi-TM mode has a reflection coefficient of 0.035 (-14.6 dB) and transmission coefficient of 0.00018 (-37.4 dB). It is worth mentioning that the reflection losses in the bimetallic rhodium–silver HPG structure is higher than that of the bimetallic rhodium–silver HPW design, as shown in Table 2.

Table 4 presents a comparison between our suggested device and those reported in the literature in terms of the study type i.e., theoretical, or experimental, TE- or TM-pass, the utilized platform, L_D , ER, IL and bandwidth. It may be seen that our suggested polarizer has a shorter L_D than those demonstrated in Xu et al. (2020), Abadía et al. (2018), Yu et al. (2019), Bai et al. (2019), Dai et al. (2020). In addition, the suggested polarizer has a better ER than those presented in Xu et al. (2020), Ying et al. (2014), Abd-Elkader et al. (2019), Kandeel et al. (2019), Bai et al. (2017), Abadía et al. (2018), Yu et al. (2019), Bai et al. (2019), Zhao et al. (2020), Dai et al. (2020). Moreover, the IL of the proposed design is lower than those reported in Ying et al. (2014), Yu et al. (2019), Bai et al. (2019), Dai et al. (2020).

Fig. 11 The calculated reflection losses of the quasi-TE and quasi-TM mode of the reported TE-pass polarizer with the wavelength. Here, a 140 nm thick layer of Si_3N_4 and Ag/Rh bimetallic structure of $h_r = 10 \text{ nm}$, $w_{m1} = 500 \text{ nm}$, $w_{m2} = 250 \text{ nm}$ and $N = 5$ are used in case of $d_{m1} = 550 \text{ nm}$ and $\eta = 0.6$

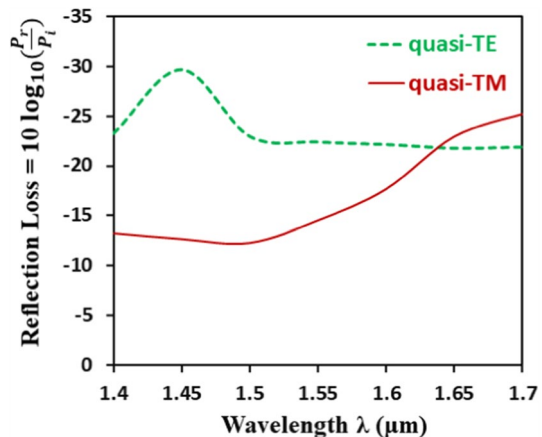


Table 4 Comparison between the suggested pass polarizer and those reported in the literature in terms of theoretical or experimental (T/E) work, TE- or TM-pass polarizer, the used platform, L_D , ER, IL, and bandwidth

Design	T/E	TE/TM	Platform	L_D (μm)	ER (dB)	IL (dB)	Bandwidth (μm)
This work	T	TE- Pass	SOI	3.5	36.6	0.8	1.4–1.7
polarizer based on HPG structure (Dai et al. 2020)	T	TE-Pass	LNOI	9	> 20	< 2.3	1.47–1.7
HPG-based polarizer (Zhao et al. 2020)	T	TM-Pass	TiO2-based	2.64	27	0.087	0.54–0.57
HPG-based polarizer (Bai et al. 2019)	E	TE-Pass	SOI	6	24–33.7	2.8–4.9	1.52–1.58
HPG-base polarizer (Yu et al. 2019)	T	TM-Pass	LNOI	23	20	2.5	1.48–1.62
polarizer based on HPW with a segmented metal design (Abadia et al. 2018)	T	TE-Pass	SOI	5.5	20	1.7	Over all the optical communication bands
HPG-based polarizer (Bai et al. 2017)	T	TM-Pass	SOI	2.5	25	0.088	1.52–1.8
Hybrid bi-metallic polarizer (Kandeel et al. 2019)	T	TE-Pass	SOI	1.5	32.7	0.13	1.54–1.7
Hybrid bi-metallic polarizer (Kandeel et al. 2019)	T	TM-Pass	SOI	2	31.5	0.17	1.54–1.7
AZO-based HP polarizer (Abd-Elkader et al. 2019)	T	TE-Pass	SOI	3	20.6	0.21	1.54–1.75
AZO-based HP polarizer (Abd-Elkader et al. 2019)	T	TM-Pass	SOI	1	22	0.11	1.49–1.75
polarizer based on a HPW (Ying et al. 2014)	T	TE-Pass	SOI	0.8	19	< 1	1.475–1.625
polarizer based on interleaved sub-wavelength gratings strip waveguide (Xu et al. 2020)	T	TM-Pass	SOI	5.2	20	0.32	1.465–1.62

The fabrication process of the proposed structure can be carried out as follows: the silicon core can be deposited on a silica wafer using electron beam lithography. The Si_3N_4 layer can be defined using plasma-enhanced chemical vapor deposition (PECVD) or low-pressure chemical vapor deposition (LPCVD) (Huang 2016). PECVD is a technique that depends on applying a plasma to produce some of the energy necessary for the deposition reaction to occur. Compared to purely thermal processing techniques like LPCVD, it has the advantage of processing at lower temperatures. In PECVD, the co-reaction of a mixture of silane, nitrogen, and ammonia gas is the most effective way to deposit Si_3N_4 (Joshi et al. 2000). In LPCVD technique, the Si_3N_4 films are deposited by the chemical reactions in gas phase of ammonia and dichlorosilane at high temperature (700–800 °C) (Joshi et al. 2000). The LPCVD is a slow deposition technique, while the PECVD has a higher deposition rate and relatively low temperatures (200–400 °C) (Joshi et al. 2000). Then, the plasmonic layers can be deposited by sputtering and using a proper lift-off process, the bimetallic grating can be fabricated.

4 Conclusion

In summary, we have proposed and investigated a compact and broadband quasi-TE pass polarizer using hybrid plasmonic grating (HPG) structure based on SOI platform. A comprehensive simulation study is accomplished to analyze the suggested structure for optimal performance. The simulation has shown that the (Ag / Rh) metal structures introduce significant coupling losses towards the plasmonic grating over several periods for the TM mode while the influence on the TE mode is very small. The suggested polarizer of 3.5 μm device length can achieve high extinction ratio of 36.6 dB and about -0.8 dB IL at an operating wavelength of 1.55 μm .

Authors' contributions B. M. Younis, Mohamed Farhat O. Hameed, and S. S. A. Obayya have proposed the idea. Ola Youssef M. Hiza has performed the simulations of the reported polarizer. All authors have contributed to the analysis, discussion, writing and revision of the paper.

Funding Open access funding provided by The Science, Technology & Innovation Funding Authority (STDF) in cooperation with The Egyptian Knowledge Bank (EKB). No fund is associated with the current manuscript.

Availability of data and materials The data will be available upon request.

Declarations

Competing interests The authors would like to clarify that there is no financial/non-financial interests that are directly or indirectly related to the work submitted for publication.

Ethical approval The authors declare that there are no conflicts of interest related to this article.

Open Access This article is licensed under a Creative Commons Attribution 4.0 International License, which permits use, sharing, adaptation, distribution and reproduction in any medium or format, as long as you give appropriate credit to the original author(s) and the source, provide a link to the Creative Commons licence, and indicate if changes were made. The images or other third party material in this article are included in the article's Creative Commons licence, unless indicated otherwise in a credit line to the material. If material is not included in the article's Creative Commons licence and your intended use is not permitted by statutory regulation or exceeds the permitted use, you will need to obtain permission directly from the copyright holder. To view a copy of this licence, visit <http://creativecommons.org/licenses/by/4.0/>.

References

- Abadía, N., et al.: CMOS-compatible multi-band plasmonic TE-pass polarizer. *Opt. Express* **26**(23), 30292–30304 (2018)
- Abd-Elkader, A.E.-S., Hameed, M.F.O., Areed, N.F.F., Mostafa, H.E.-D., Obayya, S.S.A.: Ultracompact AZO-based TE-pass and TM-pass hybrid plasmonic polarizers. *JOSA B* **36**(3), 652–661 (2019)
- Adachi, S.: *Handbook on Optical Constants of Metals, The: In Tables and Figures*. World Scientific, Singapore (2012)
- Ahmadivand, A., Sinha, R., Kaya, S., Pala, N.: Rhodium plasmonics for deep-ultraviolet bio-chemical sensing. *Plasmonics* **11**(3), 839–849 (2016)
- Alam, M., Aitchison, J.S., Mojahedi, M.: Compact hybrid TM-pass polarizer for silicon-on-insulator platform. *Appl. Opt.* **50**(15), 2294–2298 (2011)
- Alam, M.Z., Aitchison, J.S., Mojahedi, M.: Compact and silicon-on-insulator-compatible hybrid plasmonic TE-pass polarizer. *Opt. Lett.* **37**(1), 55–57 (2012)
- Azzam, S.I., Obayya, S.S.A.: Ultra-compact resonant tunneling-based TE-pass and TM-pass polarizers for SOI platform. *Opt. Lett.* **40**(6), 1061–1064 (2015)
- Azzam, S.I.H., Hameed, M.F.O., Areed, N.F.F., Abd-Elrazzak, M.M., El-Mikaty, H.A., Obayya, S.S.A.: Proposal of an ultracompact CMOS-compatible TE-/TM-pass polarizer based on SoI platform. *IEEE Photon. Technol. Lett.* **26**(16), 1633–1636 (2014b)
- Azzam, S.I.H., Areed, N.F.F., Abd-Elrazzak, M.M., El-Mikati, H.A., Obayya, S.S.A.: Compact polarization rotator based on SOI platform. In: 2014a 31st National Radio Science Conference (NRSC), pp. 288–293 (2014a).
- Babicheva, V.E., Boltasseva, A., Lavrinenko, A.V.: Transparent conducting oxides for electro-optical plasmonic modulators. *Nanophotonics* **4**(2), 165–185 (2015)
- Bai, B., Liu, L., Chen, R., Zhou, Z.: Low loss, compact TM-pass polarizer based on hybrid plasmonic grating. *IEEE Photon. Technol. Lett.* **29**(7), 607–610 (2017)
- Bai, B., Yang, F., Zhou, Z.: Demonstration of an on-chip TE-pass polarizer using a silicon hybrid plasmonic grating. *Photonics Res.* **7**(3), 289–293 (2019)
- Barwicz, T., et al.: Polarization-transparent microphotonic devices in the strong confinement limit. *Nat. Photonics* **1**(1), 57–60 (2007)
- Capretti, A., Wang, Y., Engheta, N., Dal Negro, L.: Enhanced third-harmonic generation in Si-compatible epsilon-near-zero indium tin oxide nanolayers. *Opt. Lett.* **40**(7), 1500–1503 (2015)
- Chen, J., Smolyakov, G.A., Brueck, S.R.J., Malloy, K.J.: Surface plasmon modes of finite, planar, metal-insulator-metal plasmonic waveguides. *Opt. Express* **16**(19), 14902–14909 (2008)
- Coblentz, W.W., Stair, R.: Note on the spectral reflectivity of rhodium. *J. Res. Natl. Bur. Stand.* **22**(1), 93–95 (1939)
- Dai, D., Wang, Z., Julian, N., Bowers, J.E.: Compact broadband polarizer based on shallowly-etched silicon-on-insulator ridge optical waveguides. *Opt. Express* **18**(26), 27404–27415 (2010)
- Dai, D., Bauters, J., Bowers, J.E.: Passive technologies for future large-scale photonic integrated circuits on silicon: polarization handling, light non-reciprocity and loss reduction. *Light Sci. Appl.* **1**(3), e1–e1 (2012)
- Dai, S., et al.: Broadband and compact TE-pass polarizer based on hybrid plasmonic grating on LNOI platform. *IEEE Photon. J.* **13**(1), 1–9 (2020)
- Gao, L., Huo, Y., Harris, J.S., Zhou, Z.: Ultra-compact and low-loss polarization rotator based on asymmetric hybrid plasmonic waveguide. *IEEE Photon. Technol. Lett.* **25**(21), 2081–2084 (2013)
- Gaun, X., Xu, P., Shi, Y., Dai, D.: Ultra-compact and ultra-broadband TE-pass polarizer with a silicon hybrid plasmonic waveguide. In: *Integrated Optics: Devices, Materials, and Technologies XVIII*, vol. 8988, pp. 213–219 (2014)
- Goto, H., Komata, K., Minami, S.: Impact of Pd-Rh interaction on the performance of three-way catalysts. *SAE Technical Paper* (2014)
- Gramotnev, D.K., Bozhevolnyi, S.I.: Plasmonics beyond the diffraction limit. *Nat. Photon.* **4**(2), 83–91 (2010)
- Guan, X., Wu, H., Shi, Y., Dai, D.: Extremely small polarization beam splitter based on a multimode interference coupler with a silicon hybrid plasmonic waveguide. *Opt. Lett.* **39**(2), 259–262 (2014)
- Hameed, M.F.O., Hussain, F.F.K., Obayya, S.S.A.: Ultracompact polarization rotator based on liquid crystal channel on silicon. *J. Light. Technol.* **35**(11), 2190–2199 (2017a)
- Hameed, M.F.O., Zaghoul, R., Azzam, S.I., Obayya, S.S.A.: Ultrashort hybrid plasmonic transverse electric pass polarizer for silicon-on-insulator platform. *Opt. Eng.* **56**(1), 17107 (2017b)
- Hao, W., Wang, J., Chen, L.: Plasmonic metasurfaces enabled ultra-compact broadband waveguide TM-PASs polarizer. *Ann. Phys.* **533**(1), 2000422 (2021)

- Homola, J., Yee, S.S., Gauglitz, G.: Surface plasmon resonance sensors. *Sensors Actuators B Chem.* **54**(1–2), 3–15 (1999)
- Huang, T.: TE-pass polarizer based on epsilon-near-zero material embedded in a slot waveguide. *IEEE Photon. Technol. Lett.* **28**(20), 2145–2148 (2016)
- Huang, Y., Zhu, S., Zhang, H., Liow, T.-Y., Lo, G.-Q.: CMOS compatible horizontal nanoplasmonic slot waveguides TE-pass polarizer on silicon-on-insulator platform. *Opt. Express* **21**(10), 12790–12796 (2013)
- Johnson, P.B., Christy, R.-W.: Optical constants of the noble metals. *Phys. Rev. B* **6**(12), 4370 (1972)
- Joshi, B.C., Eranna, G., Runthala, D.P., Dixit, B.B., Wadhawan, O.P., Vyas, P.D.: LPCVD and PECVD silicon nitride for microelectronics technology (2000)
- Kandeel, A.F., Hameed, M.F.O., AbdelHamid, H., Obayya, S.S.A.: CMOS-compatible hybrid bi-metallic TE/TM-pass polarizers based on ITO and ZrN. *Appl. Opt.* **58**(24), 6684–6692 (2019)
- Kurihara, K., Suzuki, K.: Theoretical understanding of an absorption-based surface plasmon resonance sensor based on Kretschmann's theory. *Anal. Chem.* **74**(3), 696–701 (2002)
- Lee, H.W., et al.: Nanoscale conducting oxide PlasMOSter. *Nano Lett.* **14**(11), 6463–6468 (2014)
- Liu, L., Ding, Y., Yvind, K., Hvam, J.M.: Silicon-on-insulator polarization splitting and rotating device for polarization diversity circuits. *Opt. Express* **19**(13), 12646–12651 (2011)
- Lumerical FDTD solutions software. www.lumerical.com/tcadproducts/fdtd/e
- Mishra, A.K., Mishra, S.K.: Gas sensing in Kretschmann configuration utilizing bi-metallic layer of Rhodium–silver in visible region. *Sensors Actuators B Chem.* **237**, 969–973 (2016)
- Mishra, S.K., Malviya, K.D., Mishra, A.K.: Highly sensitive bimetallic plasmonic sensing probe for aqueous samples. *Opt. Quantum Electron.* **52**(6), 1–10 (2020)
- Ng, T.K., Khan, M.Z.M., Al-Jabr, A., Ooi, B.S.: Analysis of CMOS compatible Cu-based TM-pass optical polarizer. *IEEE Photon. Technol. Lett.* **24**(9), 724–726 (2012)
- Ni, B., Xiao, J.: Subwavelength-grating-based compact and broadband TE-pass polarizer for slot waveguides on a SOI platform. *JOSA B* **36**(8), 2126–2133 (2019)
- Saitoh, E., Kawaguchi, Y., Saitoh, K., Koshiba, M.: TE/TM-pass polarizer based on lithium niobate on insulator ridge waveguide. *IEEE Photon. J.* **5**(2), 6600610 (2013)
- Sharma, V.K., Kumar, A., Kapoor, A.: High extinction ratio metal–insulator–semiconductor waveguide surface plasmon polariton polarizer. *Opt. Commun.* **284**(7), 1815–1821 (2011)
- Shelef, M., Graham, G.W.: Why rhodium in automotive three-way catalysts? *Catal. Rev.* **36**(3), 433–457 (1994)
- Song, Y., Xu, P.: Design of ultra-low insertion loss active transverse electric-pass polarizer based Ge₂Sb₂Te₅ on silicon waveguide. *Opt. Commun.* **426**, 30–34 (2018)
- Steinlechner, J., et al.: Optical absorption of silicon nitride membranes at 1064 nm and at 1550 nm. *Phys. Rev. D* **96**(2), 22007 (2017)
- Sun, X., Alam, M.Z., Wagner, S.J., Aitchison, J.S., Mojahedi, M.: Experimental demonstration of a hybrid plasmonic transverse electric pass polarizer for a silicon-on-insulator platform. *Opt. Lett.* **37**(23), 4814–4816 (2012)
- Sun, X., Mojahedi, M., Aitchison, J.S.: Hybrid plasmonic waveguide-based ultra-low insertion loss transverse electric-pass polarizer. *Opt. Lett.* **41**(17), 4020–4023 (2016)
- Wang, Q., Ho, S.-T.: Ultracompact TM-pass silicon nanophotonic waveguide polarizer and design. *IEEE Photon. J.* **2**(1), 49–56 (2010)
- Wang, B., Blaize, S., Salas-Montiel, R.: Nanoscale plasmonic TM-pass polarizer integrated on silicon photonics. *Nanoscale* **11**(43), 20685–20692 (2019)
- Wu, S., Xiao, J., Feng, T., Yao, X.S.: Broadband and high extinction ratio hybrid plasmonic waveguide-based TE-pass polarizer using multimode interference. *JOSA B* **37**(10), 2968–2975 (2020)
- Xie, X., Liu, F., Chen, Q., Zhang, Y.: Design of ultra-high extinction ratio TM- and TE-pass polarizers based on Si-ScO₂Sb₂Te₃ Hybrid Waveguide. *Micromachines* **13**(4), 495 (2022)
- Xu, Y., Xiao, J.: Compact and high extinction ratio polarization beam splitter using subwavelength grating couplers. *Opt. Lett.* **41**(4), 773–776 (2016)
- Xu, P., Lu, Y., Yu, Z., Dai, S.: Ultra-compact active TE and TM pass polarizers based on Ge₂Sb₂Te₅ in silicon waveguide. *IEEE Photon. Technol. Lett.* **28**(23), 2697–2700 (2016)
- Xu, Z., Lyu, T., Sun, X.: Interleaved subwavelength gratings strip waveguide based TM pass polarizer on SOI platform. *IEEE Photon. J.* **12**(2), 1–10 (2020)
- Ye, W.N., Xiong, Y.: Review of silicon photonics: history and recent advances. *J. Mod. Opt.* **60**(16), 1299–1320 (2013)
- Ying, Z., Wang, G., Zhang, X., Huang, Y., Ho, H.-P., Zhang, Y.: Ultracompact TE-pass polarizer based on a hybrid plasmonic waveguide. *IEEE Photonics Technol. Lett.* **27**(2), 201–204 (2014)

- Yu, W., Dai, S., Zhao, Q., Li, J., Liu, J.: Wideband and compact TM-pass polarizer based on hybrid plasmonic grating in LNOI. *Opt. Express* **27**(24), 34857–34863 (2019)
- Zafar, H., Khilo, A., Dahlem, M.S.: Compact silicon TE-pass polarizer using rib waveguide adiabatic bends with side gratings. In: *Integrated Photonics Research, Silicon and Nanophotonics*, pp. ITh3C-2 (2019)
- Zettsu, N., McLellan, J.M., Wiley, B., Yin, Y., Li, Z., Xia, Y.: Synthesis, stability, and surface plasmonic properties of rhodium multipods, and their use as substrates for surface-enhanced Raman scattering. *Angew Chemie* **118**(8), 1310–1314 (2006)
- Zhang, J., Cassan, E., Zhang, X.: Wideband and compact TE-pass/TM-stop polarizer based on a hybrid plasmonic Bragg grating for silicon photonics. *J. Light. Technol.* **32**(7), 1383–1386 (2014)
- Zhao, Q., Yu, W., Zhao, Y., Dai, S., Liu, J.: TiO₂-based compact TM-pass polarizer at visible wavelengths with ultra-low power loss. *Opt. Commun.* **475**, 126282 (2020)

Publisher's Note Springer Nature remains neutral with regard to jurisdictional claims in published maps and institutional affiliations.

Authors and Affiliations

Ola Youssef M. Hiza¹ · B. M. Younis^{2,3} · Nihal F. F. Areed^{1,2} ·
Mohamed Farhat O. Hameed^{2,4,5} · S. S. A. Obayya^{1,2}

¹ Faculty of Engineering, Electronics and Communications Department, Faculty of Engineering, University of Mansoura, Mansoura 35516, Egypt

² Center for Photonics and Smart Materials, Zewail City of Science, Technology and Innovation, October Gardens, 6th of October City, Giza 12588, Egypt

³ Electronics and Communications Engineering Department, Misr Higher Institute for Engineering and Technology (MET), Mansoura 35516, Egypt

⁴ Mathematics and Engineering Physics Department, Faculty of Engineering, University of Mansoura, Mansoura 35516, Egypt

⁵ Nanotechnology and Nanoelectronics Engineering Program, Zewail City of Science, Technology and Innovation, October Gardens, 6th of October City, Giza 12588, Egypt